

Two-dimensional hexagonal Zn_3Si_2 monolayer: Dirac cone material and Dirac half-metallic manipulation

Yurou Guan(官雨柔), Lingling Song(宋玲玲), Hui Zhao(赵慧), Renjun Du(杜仁君), Liming Liu(刘力铭), Cuixia Yan(闫翠霞), Jinming Cai(蔡金明)

Citation: Chin. Phys. B . 2020, 29(8): 087103 . **doi:** 10.1088/1674-1056/ab943a
Journal homepage: http://cpb.iphy.ac.cn; http://iopscience.iop.org/cpb

What follows is a list of articles you may be interested in

Ab initio calculations on oxygen vacancy defects in strained amorphous silica

Bao-Hua Zhou(周保花), Fu-Jie Zhang(张福杰), Xiao Liu(刘笑), Yu Song(宋宇), Xu Zuo(左旭)
Chin. Phys. B . 2020, 29(4): 047103 . **doi:** 10.1088/1674-1056/ab75db

Electronic properties of size-dependent $MoTe_2$/WTe_2 heterostructure

Jing Liu(刘婧), Ya-Qiang Ma(马亚强), Ya-Wei Dai(戴雅薇), Yang Chen(陈炀), Yi Li(李依), Ya-Nan Tang(唐亚楠), Xian-Qi Dai(戴宪起)
Chin. Phys. B . 2019, 28(10): 107101 . **doi:** 10.1088/1674-1056/ab3b53

Prediction of high-mobility two-dimensional electron gas at $KTaO_3$-based heterointerfaces

Fu-Ning Wang(王芙凝), Ji-Chao Li(李吉超), Yi Li(李宜), Xin-Miao Zhang(张鑫淼), Xue-Jin Wang(王学晋), Yu-Fei Chen(陈宇飞), Jian Liu(刘剑), Chun-Lei Wang(王春雷), Ming-Lei Zhao(赵明磊), Liang-Mo Mei(梅良模)
Chin. Phys. B . 2019, 28(4): 047101 . **doi:** 10.1088/1674-1056/28/4/047101

Graphene-like Be_3X_2 (X=C, Si, Ge, Sn): A new family of two-dimensional topological insulators

Lingling Song(宋玲玲), Lizhi Zhang(张礼智), Yurou Guan(官雨柔), Jianchen Lu(卢建臣), Cuixia Yan(闫翠霞), Jinming Cai(蔡金明)
Chin. Phys. B . 2019, 28(3): 037101 . **doi:** 10.1088/1674-1056/28/3/037101

Exploration of the structural and optical properties of a red-emitting phosphor $K_2TiF_6:Mn^{4+}$

Xi-Long Dou(豆喜龙), Xiao-Yu Kuang(邝小渝), Xin-Xin Xia(夏欣欣), Meng Ju(巨濛)
Chin. Phys. B . 2019, 28(1): 017107 . **doi:** 10.1088/1674-1056/28/1/017107

Two-dimensional hexagonal Zn_3Si_2 monolayer: Dirac cone material and Dirac half-metallic manipulation*

Yurou Guan(官雨柔), Lingling Song(宋玲玲), Hui Zhao(赵慧), Renjun Du(杜仁君), Liming Liu(刘力铭), Cuixia Yan(闫翠霞)†, and Jinming Cai(蔡金明)‡

Faculty of Materials Science and Engineering, Kunming University of Science and Technology, Kunming 650093, *China*

(Received 13 March 2020; revised manuscript received 18 May 2020; accepted manuscript online 19 May 2020)

The fascinating Dirac cone in honeycomb graphene, which underlies many unique electronic properties, has inspired the vast endeavors on pursuing new two-dimensional (2D) Dirac materials. Based on the density functional theory method, a 2D material Zn_3Si_2 of honeycomb transition-metal silicide with intrinsic Dirac cones has been predicted. The Zn_3Si_2 monolayer is dynamically and thermodynamically stable under ambient conditions. Importantly, the Zn_3Si_2 monolayer is a room-temperature 2D Dirac material with a spin–orbit coupling energy gap of 1.2 meV, which has an intrinsic Dirac cone arising from the special hexagonal lattice structure. Hole doping leads to the spin polarization of the electron, which results in a Dirac half-metal feature with single-spin Dirac fermion. This novel stable 2D transition-metal-silicon-framework material holds promises for electronic device applications in spintronics.

Keywords: two-dimensional (2D) Dirac cone material, Dirac half-metal, first-principles calculation, spin–orbit coupling

PACS: 71.15.Mb, 73.20.At **DOI:** 10.1088/1674-1056/ab943a

1. Introduction

Dirac materials[1] are a class of materials which possess a unique Dirac-like cone in band structure within the first Brillouin zone. Graphene, as the most typical two-dimensional (2D) Dirac material,[2] has stimulated interest in finding Dirac materials of two-dimensional crystals.[3–5] Dirac fermions produced in Dirac cone structures are different from the standard electrons of metals, whose energy has a linear dependence on momentum and follows the Dirac equation.[6] In particular, the massless fermions lead to some novel properties in graphene, such as half-integer[7,8]/fractional[9,10]/fractal[11–13] quantum Hall effects (QHE) and ultrahigh carrier mobility.[14] Compared to the single-element Dirac material, bi-element Dirac materials have more complex structures and more modulation potential. Until now, many 2D Dirac cone materials based on p-block metals or transition metal oxides have been proposed, such as Na_3Bi,[15] Bi_2Te_3/Sb_2Te_3,[16] $TlBiSe_3$,[17] $(VO_2)_n/(TiO_2)_m$, $(CrO_2)_n/(TiO_2)_m$,[18] and $Cs_3Bi_2Br_9$ bilayer.[19] Recently, the 2D transition metal-based QSH insulators M_3C_2 (M = Zn, Cd, Hg)[20] with Dirac cone have also caused interest due to their high structural stability and diversity, and their additional phases of node-line semimetal under external strain. On the other hand, organometallic crystals of $Pb_2(C_6H_4)_3$,[21] $Ni_2(C_6H_4)_3$, and $Co_2(C_6H_4)_3$.[22] with a hexagonal lattice have recently been proposed to possess Dirac cones. Moreover, due to the incorporation of the magnetic Ni and Co atoms, $Ni_2(C_6H_4)_3$ and $Co_2(C_6H_4)_3$ present half-metallic properties, which may extend the applications of 2D Dirac materials in spintronics.[23] The regulation of half-metallic (HM) properties in Dirac cone materials promotes their application in spintronics.

Recently, a family of 2D Dirac materials called Dirac half metals (DHM) has emerged which has potential applications in high-speed and low-power-consumption spintronic devices. Combining the two fascinating properties of massless Dirac fermions and 100% spin polarization, the DHM[24] was investigated based on the model of a triangular lattice. The DHM has the full bandgap in one spin channel and retains the Dirac cone in the other channel. At present, based on theoretical predictions, a large number of intrinsic DHM materials have been discovered, such as heterostructures (CrO_2/TiO_2),[25] Kagome lattices ($Ni_2C_{24}S_6H_2$, MnDCA, and $M_3C_{12}O_{12}$),[26–28] honeycomb-Kagome lattices (C_3Ca_2 and Nb_2O_3),[29,30] MXene materials (YN_2),[31] and Na_2C.[32] In addition, the gap opening by the spin–orbit coupling (SOC) drives the DHM MnX_3 (X = F, Cl, Br, I)[33] into the quantum anomalous Hall state. However, there are few reports on the manipulation of the DHM properties.

In this work, based on the density functional theory,

*Project supported by the National Natural Science Foundation of China (Grant Nos. 11674136 and 11564022), Yunnan Province for Recruiting High-Caliber Technological Talents, China (Grant No. 1097816002), Reserve Talents for Yunnan Young and Middle-aged Academic and Technical Leaders, China (Grant No. 2017HB010), the Academic Qinglan Project of KUST (Grant No. 1407840010), the Analysis and Testing Fund of KUST (Grant No. 2017M20162230010), and the High-level Talents of KUST (Grant No. 1411909425).

†Corresponding author. E-mail: cuixiayan09@gmail.com

‡Corresponding author. E-mail: j.cai@kmsut.edu.cn

© 2020 Chinese Physical Society and IOP Publishing Ltd

a novel 2D crystal in transition metal silicide Zn_3Si_2 with a hexagonal lattice has been predicted. It not only shows good stability but also exhibits interesting orbital configurations and unique electron properties. In particular, the Zn_3Si_2 monolayer demonstrates zero-gap Dirac semiconductive feature and possesses a distinct Dirac cone in the absence of SOC. When SOC is considered, the monolayer shows a gap of about 1.2 meV. Carrier doping arouses the spin-polariztion of the structure and leads to the spin splitting of the Dirac band in the case of no external magnetic field. As a result, a Dirac half-metal with single-spin Dirac fermion (SDF) can be obtained via one-hole doping. These findings render the Zn_3Si_2 monolayer a promising platform for applications in spintronic devices.

2. Method

The first principles computation is implemented in the Vienna *ab initio* simulation software package (VASP).[34,35] The projector augmented plane wave (PAW) approach is used to represent the ion–electron interaction. The Perdew–Burke–Ernzerhof (PBE) generalized gradient approximation is adopted for the electron-electron interactions.[36] To eliminate spurious interactions between periodic replicas, the Zn_3Si_2 monolayer is separated from each other in the aperiodic direction by a vacuum region of 18 Å. The energy cutoff of the plane wave is set to 400 eV. The energetic and force convergence criteria are set at 10^{-6} eV and 0.02 eV·Å^{-1}, respectively. A $13\times13\times1$ Monkhorst–Park k-point mesh is used to do the structural optimization and a $35\times35\times1$ k-point mesh for the static self-consistent calculation. The phonon dispersion relationship is calculated based on the finite displacement method in the PHONOPY code[37] combined with the VASP. Thermal stability is also examined via several *ab initio* molecular dynamics (AIMD) simulations using the Nosé algorithm[38] in the NVT ensemble at 300 K.

3. Results and discussion

3.1. Geometric structure and stability

Figure 1(a) presents the top and side views of the geometric structure of the Zn_3Si_2 monolayer, containing three zinc (Zn) atoms and two silicon (Si) atoms in a unit cell. Obviously, the Zn_3Si_2 monolayer has a planar honeycomb lattice structure with *P6/mmm* (No. 16) symmetry. The black dotted line indicates the minimum repeating unit of Zn_3Si_2 with $a=b=8.05$ Å. As shown in Fig. 1(a), there are one unique Zn atom (site symmetry $3g$) and one independent Si atom (site symmetry $2d$) in the primitive unit of the 2D Zn_3Si_2 monolayer which is structurally similar to the graphene-like honeycomb Be_3Si_2[39] monolayer. In this planar monolayer, the bond angle Si–Zn–Si is 120° and the Zn–Si bond length is 2.31 Å (as shown in Fig. 1(b)). All Si atoms are trigonally coordinated to surrounding the Zn atoms through sp^2-hybridization. Such structure can be seen as transition metal atoms been linearly interposed between two Si atoms in an enlarged silicon framework, it is a benefit to the expansion of the π bond and the stability of the 2D sheet.

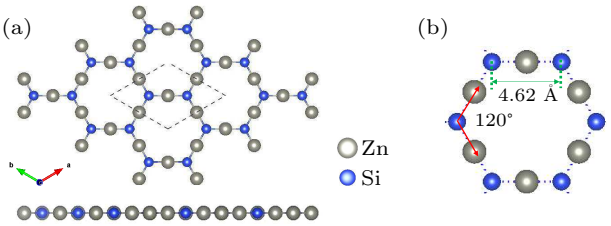


Fig. 1. (a) Optimized geometry of Zn_3Si_2 monolayer, with a unit cell labeled by the black dotted line. (b) A zoom-in figure of (a).

To examined the stability of the Zn_3Si_2 lattice, the cohesive energy[40] with respect to the isolated atoms is first considered, which is obtained as $E_{\rm coh}=(3E_{\rm Zn}+2E_{\rm Si}-E_{\rm Zn_3Si_2})/5=1.95$ eV per atom, where $E_{\rm Zn_3Si_2}$, $E_{\rm Zn}$, and $E_{\rm Si}$ are the total energy of the monolayer, the energy of a single zinc atom, and the energy of a silicon atom, respectively. The cohesive energy in our result indicates that the Zn_3Si_2 monolayer might be synthesized by epitaxial growth on an appropriate substrate such as silicone, because the value is comparable with that of grey antimonene (2.30 eV/atom)[41] and metallic bismuthene (2.26 eV/atom).[42] In addition, the formation enthalpy also has been considered to investigate the stability of the Zn_3Si_2 lattice further according to the formula $\Delta H(Zn_3Si_2)=E(Zn_3Si_2)-[1-x]E(Zn)+xE(Si)$,[43,44] where $E(Zn_3Si_2)$ is the total energy of Zn_3Si_2 phase per atom and obtained by the first-principles calculations. E(Zn) and$E$(Si) are the energies of the pure elements Zn and Si, respectively. x is the composition of Si in the compound, $x=\frac{2}{3+2}=\frac{2}{5}$. It is found $\Delta H=-7.3$ eV, which implies that the thermal stability of Zn_3Si_2 is good.

The dynamical properties of the 2D Zn_3Si_2 monolayer have been studied by phonon dispersion calculations, as shown in Fig. 2(a). It clearly shows that the 2D Zn_3Si_2 monolayer has no imaginary frequency, indicating that the 2D Zn_3Si_2monolayer is kinetically stable. Additionally, we also perform AIMD simulations using a supercell of 3×3 unit cells (see Fig. 2(b)). Note that the structure still maintains the 2D lattice shape throughout a 3 ps MD simulation at 300 K, indicating that the Zn_3Si_2 monolayer is dynamically and thermally stable at room temperature. Considering that many 2D materials such as graphene, MoS_2, BN, and stanene have been experimentally synthesized, it is expected that a similar method can be used to synthesize a Zn_3Si_2 monolayer.

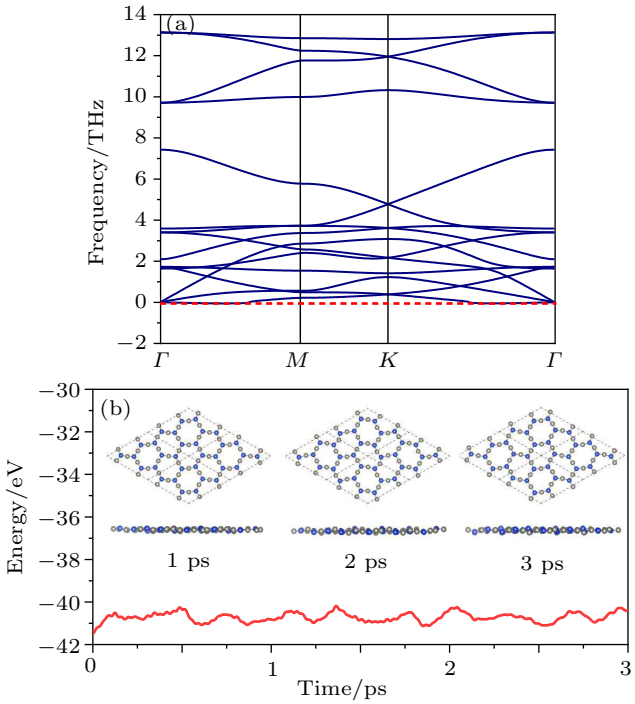


Fig. 2. (a) Phonon dispersion of Zn_3Si_2 monolayer, where no soft mode is found. (b) The total energy for the Zn_3Si_2 lattice as a function of simulation time at 300 K. The inset illustrates the snapshots of the optimized crystal structures of the Zn_3Si_2 lattice at 1 ps, 2 ps, and 3 ps.

3.2. Electronic properties and Dirac states

The chemical bonding in the monolayer can be explained by the electron localization function (ELF),[45] the charge density difference, and the partial charge densities at the Fermi level for this material (as shown in Fig. 3). The charge density difference in Fig. 3(a) shows the hole density near the zinc positions, while the electron is abundant around the in-plane orbitals of silicone, especially along the Zn–Si bonds. The electron density responsible for the formation of bonds is shifted toward the Si atoms. The shape of the distribution in the Zn_3Si_2 monolayer implies that the in-plane orbitals participate in σ-bond formation. The ELF diagram (Fig. 3(b)) shows that the electrons in Zn_3Si_2 monolayer are localized at the Si atoms, whereas the Zn atoms reveal electrons deficiency. The form of electron localization shows the sp^2 hybridization of the silicone atomic orbitals, which participates in the construction of the σ bonds. Moreover, a small part of the electron density is located in the gap region – TM donates electrons to the metalloid and then a portion of the charge is transferred from the metalloid to the gap region – revealing the characteristics of metalloid bonding. In real space, the partial charge density of the valence band (VB) maximum (Fig. 3(c)) and conductive band (CB) minimum (Fig. 3(d)) confirms that the Zn p_z, $d_{xz,yz}$, and Si p_z orbitals participate in the formation of the Dirac point. It can further stabilize the 2D framework structure of Zn_3Si_2.

To evaluate the electronic properties of the predicted monolayer Zn_3Si_2, the projected band structure and the corresponding partial density of states (PDOS) are investigated in the absence of SOC, as shown in Figs. 4(a) and 4(b). The Zn_3Si_2 monolayer is a zero-band-gap semi-metal with the VB and CB touching each other at the K point (Fig. 4(a)). The yellow, gray, blue, and green dots represent the total p_z, p_y, p_x, and d orbitals, respectively. It can be clearly seen that

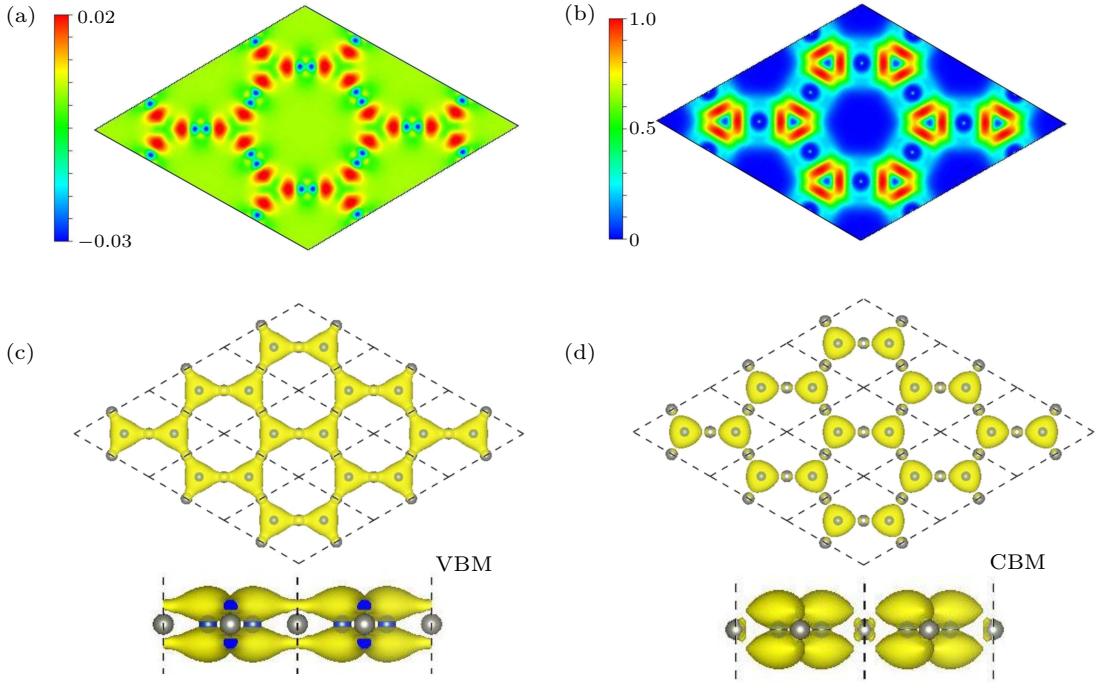


Fig. 3. (a) The charge density difference with an isovalue of 0.02 $e/\text{Å}^{-3}$. The blue and orange mean electron accumulation region and electron depletion region, respectively. (b) ELF of Zn_3Si_2 monolayer with an isovalue of 0.03 $e/\text{Å}^{-3}$. (c), (d) Top and side views of VB maximum and CB minimum charge density contours at the Dirac point of Zn_3Si_2 monolayer, respectively.

the Dirac point near the Fermi level is mainly contributed by the p_z orbitals. The other two crossing bands are mainly composed of the p_y orbital, which are about 0.5–3.5 eV below the Fermi level. Considering the D_{6h} point group symmetry of the Zn_3Si_2 monolayer, the Zn-d orbital can be divided into three categories: d_{xy,x^2-y^2}, $d_{xz,yz}$, and d_z^2. In Fig. 4(b) we plot the PDOS of the Si and Zn atoms, respectively. Near the Fermi levels, the VB and CB are mainly from the Si p_z orbital and the Zn $p_{x,y}$, $d_{xz,yz}$ orbitals, respectively. Meanwhile, the VB-1 is primarily derived from the Si $p_{x,y}$ and Zn $p_{x,y}$, d_{xy,x^2-y^2} orbitals. So, it is considered that the Dirac cone is derived from the special hexagonal lattice structure. As the Zn_3Si_2 monolayer has a planar structure, it is considered that $p_{x,y}$ and d_{xy,x^2-y^2} are hybridized to form an σ bond, while p_z and $d_{xz,yz}$ are hybridized to form a π bond. The three-dimensional (3D) valence and conduction bands are also presented in Fig. 4(c), which clearly shows the features of the Dirac cone at its high symmetry K point. The Dirac cone-like electronic states generally mean excellent electronic transport properties. We have calculated the Fermi velocity (V_F) of the Zn_3Si_2 monolayer near the Dirac point by using the equation $V_F = \partial E/(\hbar \partial k)$. The calculated V_F values along the directions $\Gamma \rightarrow K$ and $K \rightarrow M$ are 2.85×10^5 m·s^{-1} and 1.65×10^5 m·s^{-1} (without SOC calculation), respectively, which are in the same order of those of graphene (9.5×10^5 m·s^{-1} and 8.2×10^5 m·s^{-1}). The corresponding V_F values with SOC are 2.79×10^5 m·s^{-1} and 1.49×10^5 m·s^{-1}, respectively, which are similar to the results without SOC.

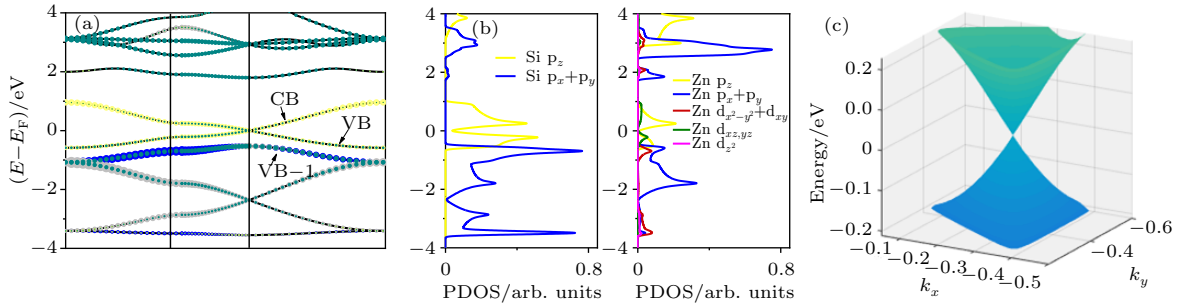


Fig. 4. The electronic properties of Zn_3Si_2 without SOC. (a) The orbital-resolved band structures for Zn_3Si_2 monolayer (yellow: total p_z orbitals; light grey: total p_y orbitals; blue: total p_x orbitals; olive: total d orbitals). The Fermi level is set to zero. (b) Projected density of states of Zn_3Si_2 monolayer. (c) 3D projection of Dirac cone in the vicinity of the K point.

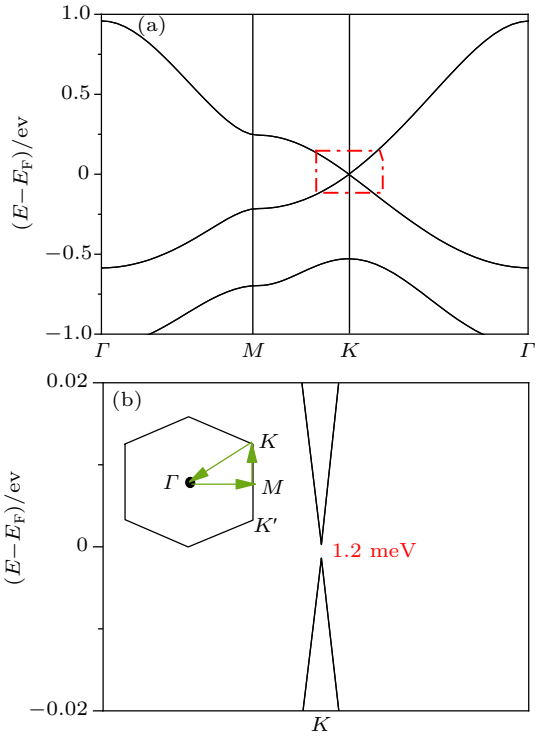


Fig. 5. (a) The calculated band structures of Zn_3Si_2 monolayer with SOC. The Fermi level is set to zero. (b) The zoom-in around the Fermi level corresponding to the red dotted box in (a), where the inset indicates the first Brillouin zone.

The SOC results in "frivolous" splitting of orbital energy levels caused by the interaction of particles' spin and orbital momentum. The band structure calculated with SOC is shown in Fig. 5(a) It can be seen that the Dirac cone remains. In Fig. 5(b), the zoom-in around Fermi energy shows that a tiny band gap of 1.2 meV appears after considering SOC. Although the crystal lattice of silicene is smaller than that of Zn_3Si_2, the bandgap of silicene (1.55 meV) with SOC is slightly larger than that of Zn_3Si_2 due to 2D silicene materials being undulating and the in-plane p_x and p_y orbitals enhancing the SOC effect.

4. Manipulation of the Dirac half-metal

According to the previous studies,[46] carrier doping is used as an effective means to manipulate the electronic structure and magnetic properties. The effect of carrier doping on the Zn_3Si_2 monolayer has been studied. It can be seen from Fig. 6(a) that the highest carrier doping concentration is 0.3 electron/hole per atom (carrier density 1.5×10^{15} cm^{-2}). This concentration is experimentally feasible through the electrolysis gates,[47] which can modulate the carrier density to 10^{15} cm^{-2} order. The negative and positive values on the horizontal ordinate are for the hole and electron dopings, respectively. It is noted that there is a transition from spin non-polarization to spin polarization through carrier doping in the

Zn_3Si_2 monolayer. It is interesting to note that the Dirac half-metallic property is shown in the case of 0.2 hole/atom doping. The band structure of the system with the doping of 0.2 hole/atom is shown in Fig. 6(b). Two fascinating properties, which are independent of the exchange-correlation functional, are observed: (1) the spin-up channel hosts a Dirac cone state at a high-symmetry K point in the vicinity of the Fermi level; (2) the spin-down channel is a semiconductor with a indirect gap of 0.71 eV (shown by a blue arrow in Fig. 6(b)). It is considered that the Fermi energy shifts below the spin-up band, such that the spin-down band is fully occupied, resulting in a truly single-spin Dirac fermion state with 100% spin-polarized currents. Our results indicate that the total magnetic moment of the Zn_3Si_2 monolayer is 1.009 μ_B. However, with the same electron doping concentration, the band splitting of the Zn_3Si_2 single layer is not very obvious (Fig. 6(c)), and the corresponding DHM is not obtained. It means that the spin-polarized Dirac electrons can be obtained by the hole doping even if there is no external magnetic field, which is a unique magnetic phenomenon of Dirac bands.

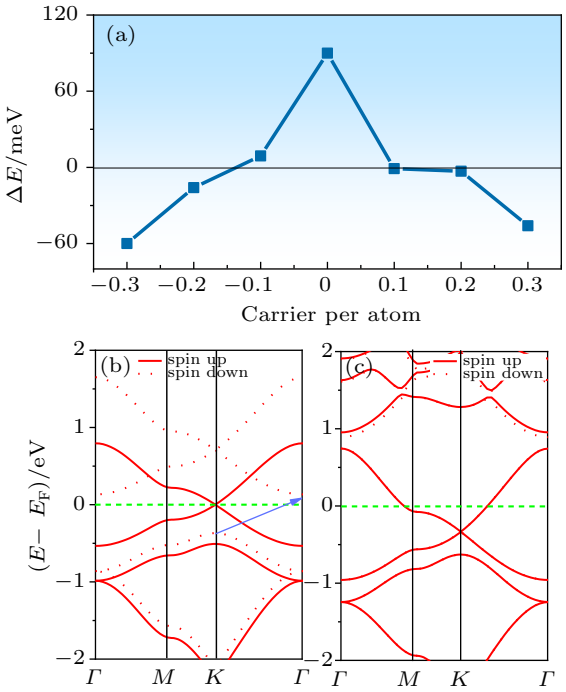


Fig. 6. (a) The $\Delta E = E_{\text{(spin-polarized)}} - E_{\text{(spin-nonpolarized)}}$ with respect to carrier doping calculated in the Zn_3Si_2 monolayer. The negative and positive values on the horizontal ordinate are for the hole and electron dopings, respectively. (b), (c) Spin-polarized band structures in the absence of SOC with the doping concentration of 0.2 hole per atom and 0.2 electron per atom, respectively.

5. Conclusion

In summary, our first-principles calculations predict the Zn_3Si_2 monolayers to be a new 2D material with intrinsic Dirac states in a hexagonal lattice. The AIMD simulations and phonon spectra reveal that the monolayer is dynamically and thermodynamically stable under ambient conditions. The Dirac cones at a point of high symmetry in the Zn_3Si_2 monolayer are sorely derived from the Si p_z and Zn p_z, $d_{xz,yz}$ orbitals, which are robust against SOC. It has a 1.2 meV SOC energy gap. Carrier doping of the monolayer leads to structural magnetism, which also induces spin-polarized Dirac electrons without an external magnetic field. In particular, the Dirac half-metallic structures are obtained when 0.2 hole/atom is doped, resulting in a single-spin Dirac fermion state with 100% spin-polarized currents. By the prediction of this novel stable 2D transition-metal-silicon-framework material, we provide a feasible strategy for the design of Dirac materials, which holds promise applications in spintronics.

References

[1] Wehling T, Black-Schaffer A M and Balatsky A V 2014 *Adv. Phys.* **63** 1
[2] Castro Neto A H, Peres N M R, Novoselov K S and Geim A K 2009 *Rev. Mod. Phys.* **81** 109
[3] Liu C C, Feng W X and Yao Y G 2011 *Phys. Rev. Lett.* **107** 076802
[4] Cahangirov S, Topsakal M, Aktürk E, Şahin H, and Ciraci S 2009 *Phys. Rev. Lett.* **102** 236804
[5] Zhu F F, Chen W J, Xu Y, Gao C L, Guan D D, Liu C H, Qian D, Zhang S C and Jia J F 2015 *Nat. Mater.* **14** 1020
[6] Novoselov K 2007 *Nat. Mater.* **6** 720
[7] Novoselov K S, Geim A K, Morozov S, Jiang D, Katsnelson M I, Grigorieva I, Dubonos S and Firsov A A 2005 *Nature* **438** 197
[8] Zhang Y, Tan Y W, Stormer H L and Kim P 2005 *Nature* **438** 201
[9] Bolotin K I, Ghahari F, Shulman M D, Stormer H L and Kim P 2009 *Nature* **462** 196
[10] Du X, Skachko I, Duerr F, Luican A and Andrei E Y 2009 *Nature* **462** 192
[11] Dean C R, Wang L, Maher P, Forsythe C, Ghahari F, Gao Y, Katoch J, Ishigami M, Moon P and Koshino M 2013 *Nature* **497** 598
[12] Ponomarenko L, Gorbachev R, Yu G, Elias D, Jalil R, Patel A, Mishchenko A, Mayorov A, Woods C and Wallbank J 2013 *Nature* **497** 594
[13] Hunt B, Sanchez-Yamagishi J, Young A, Yankowitz M, LeRoy B J, Watanabe K, Taniguchi T, Moon P, Koshino M and Jarillo Herrero P 2013 *Science* **340** 1427
[14] Bolotin K I, Sikes K J, Jiang Z, Klima M, Fudenberg G, Hone J, Kim P and Stormer H 2008 *Solid State Commun.* **146** 351
[15] Hellerstedt J, Yudhistira I, Edmonds M T, Chang L and Fuhrer M S 2017 *Phys. Rev. Mater.* **1** 054203
[16] Dil J H, Al E, Osterwalder J, Patthey L and Meier F 2009 *Phys. Rev. Lett.* **103** 146401
[17] Sato T, Segawa K, Guo H, Sugawara K and Ando Y 2010 *Phys. Rev. Lett.* **105** 136802
[18] Li X, Zhang F, Niu Q and Feng J 2014 *Sci. Rep.* **4** 6397
[19] Chen Xue Jiao L L, Shen Dezhen 2019 *Chin. Phys. B* **28** 77106
[20] Liu P F, Zhou L J, Tretiak S and Wu L M 2017 *J. Mater. Chem. C* **5** 9181
[21] Wang Z F, Liu Z and Liu F 2013 *Nat. Commun.* **4** 1471
[22] Ma Y, Dai Y, Li X, Sun Q and Huang B 2014 *Carbon* **73** 382
[23] Ma Y, Dai Y, Wei W, Huang B B and Whangbo M H 2014 *Sci. Rep.* **4** 7297
[24] Ishizuka H and Motome Y 2012 *Phys. Rev. Lett.* **109** 237207
[25] Cai T Y, Li X, Wang F, Ju S, Feng J and Gong C D 2015 *Nano Lett.* **15** 6434
[26] Wei L, Zhang X M and Zhao M W 2016 *Phys. Chem. Chem. Phys.* **18** 8059
[27] Ji W X, Zhang B M, Zhang S F, Zhang C W, Ding M, Li P and Wang P J 2017 *J. Mater. Chem. C* **5** 8504
[28] Wu M H, Wang Z J, Liu J W, Li W B, Fu H H, Sun L, Liu X, Pan M H, Weng H M and Dincă M 2017 *2D Mater.* **4** 015015
[29] Zhang S J, Zhang C W, Zhang S F, Ji W X, Li P, Wang P J, Li S S and Yan S S 2017 *Phys. Rev. B* **96** 205433
[30] He J, Ma S, Lyu P and Nachtigall P 2016 *J. Mater. Chem. C* **4** 2518

[31] Liu Z F, Liu J Y and Zhao J J 2017 *Nano Res.* **10** 1972
[32] Ji W X, Zhang B M, Zhang S F, Zhang C W, Ding M, Wang P J and Zhang R Q 2018 *Nanoscale* **10** 13645
[33] Sun Q L and Kioussis N 2018 *Phys. Rev. B* **97** 094408
[34] Kresse G and Hafner J 1993 *Phys. Rev. B* **47** 558
[35] Kresse G and Joubert D 1999 *Phys. Rev. B* **59** 1758
[36] Perdew J P, Burke K and Ernzerhof M 1998 *Phys. Rev. Lett.* **80** 891
[37] Parlinski K, Li Z and Kawazoe Y 1997 *Phys. Rev. Lett.* **78** 4063
[38] Nosé S 1984 *J. Chem. Phys.* **81** 511
[39] Song L L, Zhang L Z, Guan Y R, Lu J C, Yan C X and Cai J M 2019 *Chin. Phys. B* **28** 037101
[40] Liu P F, Zhou L, Frauenheim T and Wu L M 2016 *Phys. Chem. Chem. Phys.* **18** 30379
[41] Zhang S L, Xie M Q, Li F Y, Yan Z, Li Y F, Kan E J, Liu W, Chen Z F and Zeng H B 2016 *Angew. Chem.* **55** 1666
[42] Pumera M and Sofer Z 2017 *Adv. Mater.* **29** 1605299
[43] Liu Z R, Chen J H, Wang S B, Yuan D W, Yin M J and Wu C L 2011 *Acta Mater.* **59** 7396
[44] Wolverton C and Ozoliņš V 2006 *Phys. Rev. B* **73** 144104
[45] Savin A, Nesper R, Wengert S and Fässler T F 1997 *Angew. Chem.* **36** 1808
[46] Wang C, Zhou X, Pan Y, Qiao J, Kong X, Kaun C C and Ji W 2018 *Phys. Rev. B* **97** 245409
[47] Javey A, Guo J, Farmer D B, Wang Q, Wang D, Gordon R G, Lundstrom M and Dai H 2004 *Nano Lett.* **4** 447